ACS OMEGA

Open Access

http://pubs.acs.org/journal/acsodf

Article

Photoresponsive Nanoarchitectonics Based on Copper-Porphyrins for Near-Infrared-Enhanced Bacterial Treatment

Jing-Jing Liu, Jun Wang, Qiu-Yun Chen,* Feng Chen, and Gao-Ji Wang

Cite This: *ACS Omega* 2024, 9, 24513−24519

Read Online

ACCESS | Metrics & More | Article Recommendations | Supporting Information

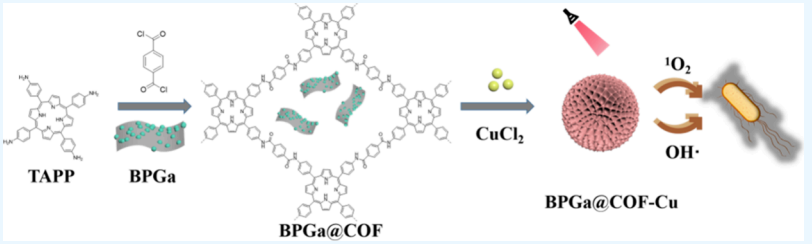

ABSTRACT: Antibiotic resistance is one of the biggest challenges that causes incurable diseases and endangers public health. Metal-porphyrin-modified nanoarchitectonics can enhance the bacterial affinity and destruction of cell walls. Herein, a new photoresponsive nanoarchitectonics (BPGa@COF-Cu) was synthesized by doping Ga(III) on the surface of black phosphorus (BP) and subsequently loaded into a Cu(II)-based covalent-organic framework (COF-Cu). The COF-Cu was induced by the coupling reaction of terephthalic chloride with amino-substituted porphyrin derivatives (THPP), followed by the coordination of the Cu(II) ion. The material BPGa@COF-Cu is a nanoball, and the mean radius is ca. 250 nm. The photochemical properties of BPGa@COF-Cu show that it efficiently catalyzes H_2O_2 into ·OH. BPGa@COF-Cu can also produce both singlet oxygen and heat upon 808 nm irradiation. Further, BPGa@COF-Cu was employed to inhibit bacteria, and the results showed that it can destroy the membrane of *bacteria*. The MIC (minimal inhibition concentration) of BPGa@COF-Cu against *E. coli* was 1 μg/mL. All the data suggest that BPGa@COF-Cu is a multiple nanoarchitectonics for bacterial treatment.

INTRODUCTION

The overuse of antibiotics causes drug resistance and biosafety issues.[1] Regarding these issues, the development of photoresponsive compounds for bacterial treatment has garnered significant attention from researchers from different disciplines.[2,3] Photodriven therapy, majorly relying on reactive oxygen generated from the reaction of O_2 and photoresponsive compounds, was used as a physio-chemical method for the treatment of drug-resistant bacteria.[4] For this reason, porphyrin derivatives, which were used for photodynamic therapy (PDT) with high singlet oxygen ($^1O_2$) generation capacity,[5] have been employed as a powerful near-infrared (NIR)-responsive lipophilic photosensitizer for DNA oxidation and bacterial inhibition.[6,7] However, the hypoxic environment and nontargeted damage to normal cells have limited their further application. The functional porphyrin showed both PDT and photothermal (PTT) effects for bacterial treatment.[8] Nanolization of porphyrins is a preferred approach, and nanometallic porphyrins exhibiting improved NIR-driven interconversion of O_2 to $^1O_2$, enabling both PDT and PTT, have been employed in the treatment of bacterial infections.[9−11] However, challenges remain in PDT and PTT therapy against pathogenic infections while side effects are avoided on normal tissues. Therefore, molecules that interfere with central metabolisms may provide a potential pathway to circumvent such issues.[12]

The metabolism of *Staphylococcus aureus* (*S. aureus*), with upregulated glyoxylate during bacterial infections, is closely related to the lipoproteins and the tricarboxylic acid cycle.[13,14] Recently, we discovered that the attenuation of pyruvic acid levels and lipase in bacteria through metal-porphyrin-doped black phosphorus (BP), combined with properties of PTT and PDT, afford a new and effective method for the inhibition on *S. aureus*.[15] Porphyrin-based metal−organic frameworks can be synthesized using a polymer (polypyrrole) core-templated method.[16] Nanoporphyrins with a polycrystalline structure can disrupt the protective layer of the bacterial membrane and attenuate bacterial metabolism.[17,18] The architecting of functional nanoporphyrins with PDT, PTT, and so forth properties can produce nanoarchitectonics (functional material systems), which would be multiple materials for bacterial membrane damage and photodriven therapy.[19] Moreover,

Received: January 15, 2024
Revised: April 15, 2024
Accepted: May 15, 2024
Published: May 27, 2024

Scheme 1. Synthesis of BPGa@COF-Cu and Inhibition Mechanism Diagram

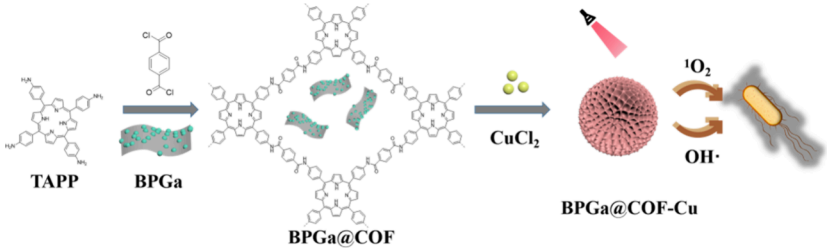

metal-porphyrin-modified nanoarchitectonics can enhance the bacterial affinity and destruction of cell walls due to the hydrophobic positively charged polycrystalline surface.[20] Biocomparable BP can be converted to phosphate species for bacterial ablation.[21,22] Meanwhile, metal-doped BP can catalyze H_2O_2 to generate hydroxyl radicals for bacterial eradication in hypoxic conditions.[17] Therefore, the combination of metal-doped BP and porphyrin-based nanoarchitectonics presents an effective method for bacterial infection treatment in low oxygen environments.

Iron-containing heme is involved in bacterial infection and glycolysis.[23] Ga(III) can be a competitor of iron ions to bind with heme biomolecules, making the iron absorption system abnormal during the bacterial infection process.[11] Ga(III) doped BP can release Ga(III) ions and oxidized BP (PO_4^{3-}) species to attenuate the bacterial metabolism.[24] Herein, Ga(III) doped BP was used as a template to direct the covalent conjugation of porphyrin (TAPP) with terephthalic chloride producing nanoporphyrin (labeled as BPGa@COF). The further coordination of BPGa@COF with Cu(II) resulted in metal−organic balls (BPGa@COF-Cu, Scheme 1). These copper-porphyrin metal−organic balls show good photothermal properties and can catalyze H_2O_2 into ·OH radicals. The MIC of BPGa@COF-Cu against *E. coli* was found to be 1 μg/mL under red LED light.

MATERIALS AND METHODS

Materials and Instruments. NANJING Xianfen-NANO Mater-Tech. Co., Ltd. (China) supplied the BP flake. Methylene blue trihydrate (MB), 1,3-diphenylisobenzofuran (DPBF), anhydrous gallium(III) chloride ($GaCl_3$), and $CuCl_2$ were obtained from Energy Chem Co. Ltd. (China). Yan-Shen Chem. Co., Ltd. provided 5,10,15,20-tetra(4-aminophenyl)-porphyrin (TAPP) and terephthalic chloride. FT-IR (Fourier transform infrared) spectra were recorded at 25 °C using a Nicolet IS50 FTIR spectrometer. Microscopes (JSM-7001F) were used for both STEM (scanning transmission electron microscopy) and EDX (energy-dispersive X-ray) spectroscopy. Raman data were collected with a Raman spectrometer (DXR, America). Photothermal data were captured by using a thermometer (TES1310). Fluorescence (or UV−vis) spectroscopic analyses were conducted using a CaryEclipse fluorescence-spectrophotometer (Australia) (or UV 3600 Plus spectrophotometer), respectively. Strains of *E. coli* (*Escherichia coli*) and *Staphylococcus aureus* (*S. aureus*), specifically standard strains ATCC25922 and CMCC26003, were procured from Shang-Hai Lu-Wei Tech. Co., Ltd.

Synthesis of BPGa@COF. $GaCl_3$ (17.6 mg, 0.1 mmol) and BP(3.2 mg, 0.1 mmol) were dispersed in CH_3CN (10 mL), then the mixture was purged with N_2 gas. The dispersion was sonicated for 12 h and centrifuged at 8000 rpm for 10 min to get black solids (BPGa, 12 mg). Next, BPGa (12 mg) in THF (6 mL) was mixed with TAPP (0.15 mmol, 101 mg) under N_2. Thereafter, terephthalic chloride (0.3 mmol, 60 mg) was added, and the dispersion was stirred at 25 °C for 12 h. Red particles BPGa@COF (100 mg) were obtained after centrifugation and washed with THF.

Synthesis of BPGa@COFCu. BPGa@COF (50 mg) and $CuCl_2$ (30 mg) were dispersed in DMF (30 mL). The dispersion was stirred under N_2 gas for 8 h at 100 °C. After cooling to 25 °C, it was centrifuged at 8000 rpm for 10 min, and purified by washing with DMF and CH_3CH_2OH, producing brick red flakes BPGa@COF-Cu (60 mg).

Quantification of Singlet Oxygen and Hydroxyl Radicals. Singlet Oxygen Detection: Using DPBF as the trapping agent, the level of $^1O_2$ was determined through UV−vis spectroscopy. A mixture containing an 8 μM DPBF solution in DMSO and a 10 μM solution of BPGa@COF and BPGa@COF-Cu was subjected to analysis. Absorbance changes at 414 nm were recorded every 5 min while being illuminated by a red LED light source with an intensity of 4 mW.

Detection of Hydroxyl Radicals. H_2O_2 (0.5 M, 20 μL) was added to the MB solution of water (1 mg/mL, 3 mL) (control group) and MB in water (1 mg/mL, 3 mL) + sample

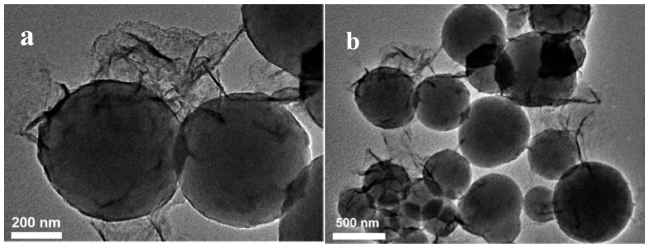

Figure 1. TEM images of BPGa@COF-Cu.

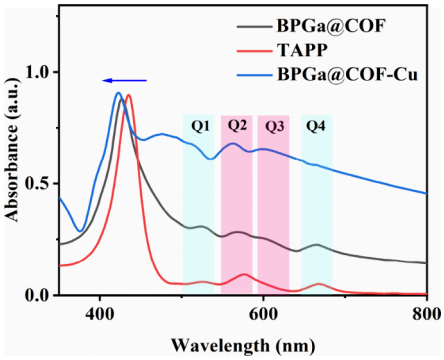

Figure 2. UV−vis spectra of TAPP (10 μg/mL), BPGa@COF (50 μg/mL), and BPGa@COF-Cu (50 μg/mL) in DMF solution.

https://doi.org/10.1021/acsomega.4c00496
ACS Omega 2024, 9, 24513−24519

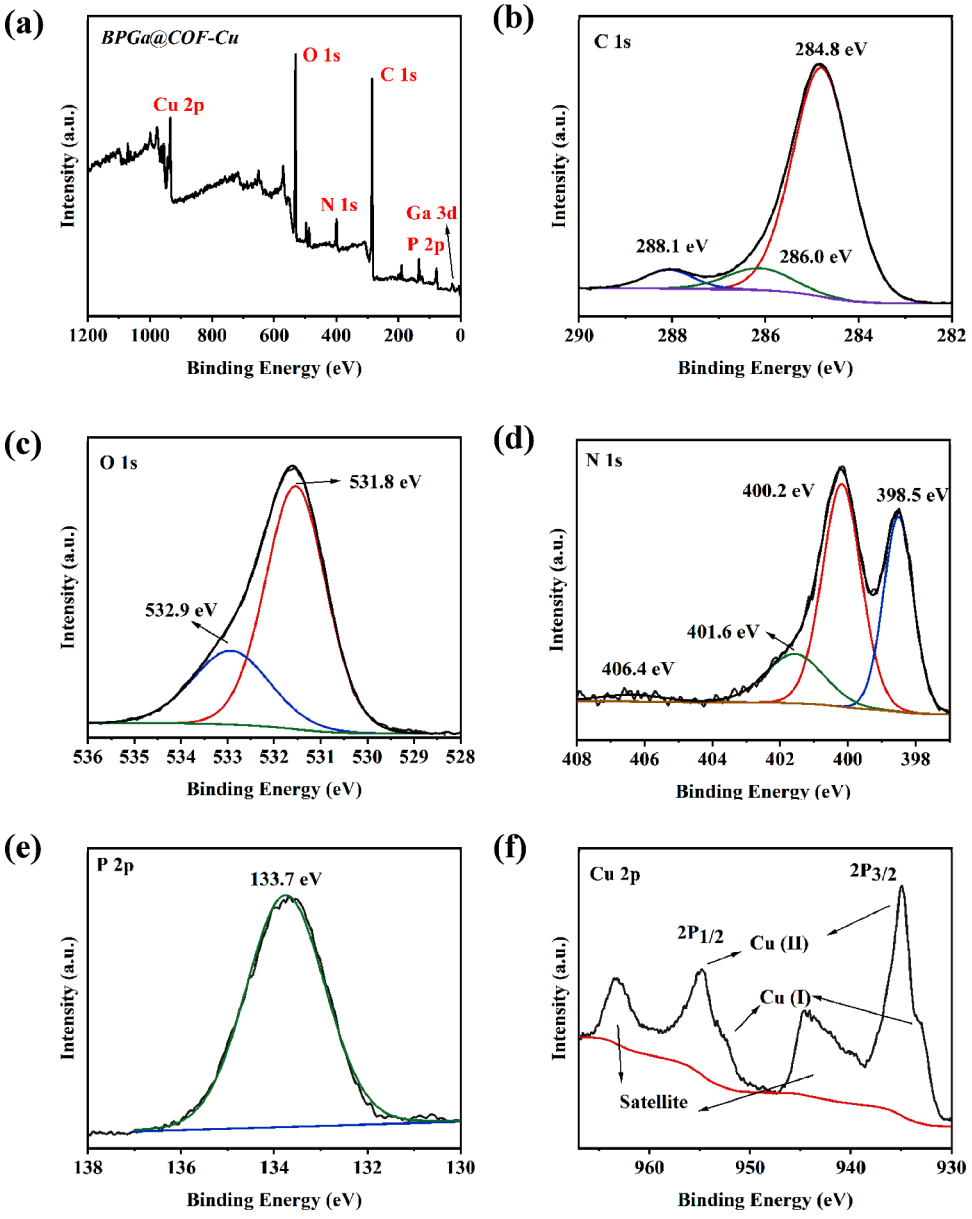

Figure 3. XPS spectra of elements in BPGa@COF-Cu (a), C 1s (b), O 1s (c), N 1s (d), P 2p (e), and Cu 2p (f).

(1 mg). After the dispersion was stirred for 10 min without or with LED (4 mW) light irradiation, the absorption change of MB at 660 nm was detected by a UV−vis spectrometer.

Photothermal Conversion Experiments. BPGa@COF-Cu was prepared in deionized water at specific concentrations (0, 25, 50, and 100 μg/mL). Subsequently, each solution (3 mL) was exposed to a NIR laser (808 nm, 2 W/cm^2) for 10 min. A digital thermometer was employed to measure the temperature of the solutions at 30-s intervals.

Antibacterial Activity. The antibacterial efficacy of BPGa@COF-Cu on the proliferation inhibition of both *E. coli* and *S. aureus* was taken through a series of controlled experiments. Initially, the bacteria in the broth were cultured at 37 °C under continuous shaking for 24 h, followed by centrifugation to collect the bacteria, which were then washed three times with deionized water. The absorption at 600 nm (OD_{600}) was recorded by UV−vis spectroscopy to calculate bacterial concentrations. For experimental procedures, 300 μL of bacterial suspension (10^6 CFU/mL) and varying concentrations of BPGa@COF-Cu (0, 10, 20, 30, 40, 50, and 100 μg/mL) were prepared. The mixtures of sample and bacteria were incubated at 37 °C for 2 h. Subsequently, each mixture (200 μL) was put onto LB agar plates. Additionally, some samples underwent further treatment involving either a 10 min exposure to a NIR laser (808 nm, 2 W/cm^2) or a 2 h exposure to red light (600−700 nm). The plates were then examined to count bacterial colonies, quantifying the antibacterial properties of BPGa@COF-Cu under various conditions.

Bacterial Morphological Changes Following Various Treatments. The changes in bacteria exposed to BPGa@COF-Cu were examined by using a scanning electron microscope (SEM). Initially, bacteria at a concentration of 10^9 CFU/mL were mixed with 100 μg/mL of BPGa@COF-Cu and subjected to a 10 min NIR laser irradiation followed by 2 h under red light (660 nm). A control group included bacteria without any irradiation. Post-treatment, the bacteria were collected via centrifugation, rinsed repeatedly with PBS, and

https://doi.org/10.1021/acsomega.4c00496
ACS Omega 2024, 9, 24513−24519

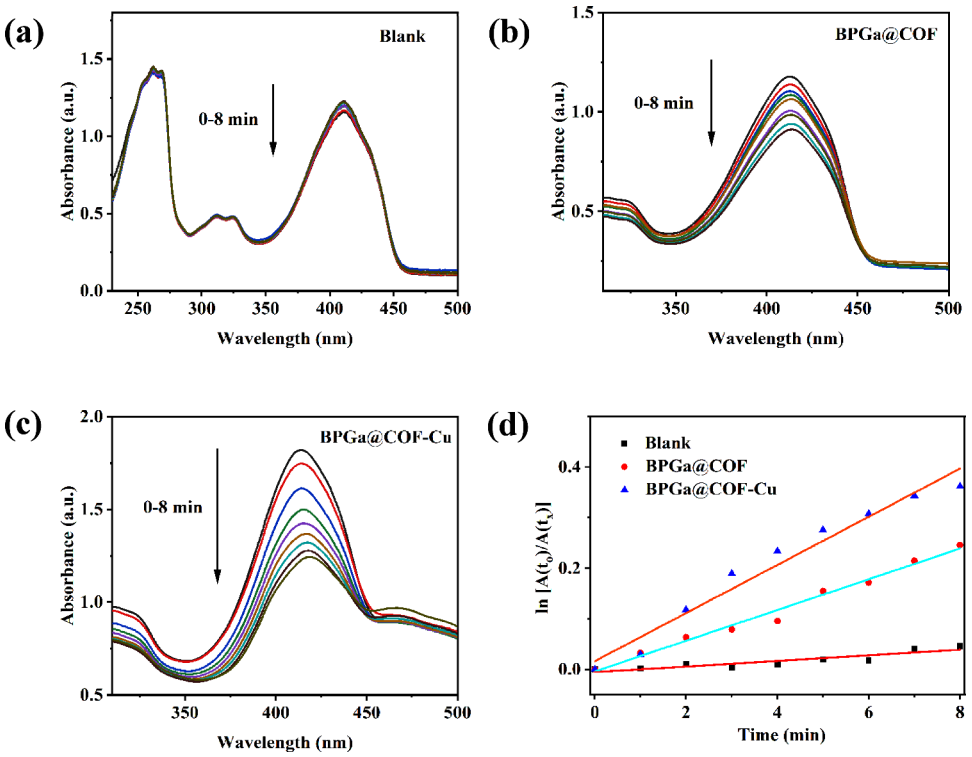

Figure 4. DPBF degradation rate in 0−8 min of blank (a), BPGa@COF (b), BPGa@COF-Cu (c), and degradation rate comparison curve (d); concentration of compound was at 10 μg/mL and the DPBF was initially at 5 × 10^{-5} M in acetonitrile.

fixed in 2.5% glutaraldehyde for 12 h. For SEM preparation, the fixed samples underwent further centrifugation and were finally resuspended in ethanol.

RESULTS AND DISCUSSION

Synthesis and Characterization of BPGa@COFCu. Initially, BPGa species were synthesized through the coordination of either BP or oxidized black phosphorus (PO_4^{3-}) with Ga(III) ions. Subsequently, BPGa served as a template for constructing a covalent-organic framework (COF), achieved via the formation of CO-NH bonds between TAPP and terephthalic chloride. This process resulted in the formation of BPGa@COF. Finally, BPGaCOF-Cu, conceptualized as metal−organic spheres, was synthesized by coordinating Cu(II) ions with the porphyrin units within BPGa@COF (Scheme 1).

TEM data showed that BPGa@COF-Cu are nanoballs with a mean radius of 250 nm (Figure 1). The −CO−NH bonds in both BPGa@COF and BPGa@COF-Cu were confirmed by the IR peak at 1667 cm^{-1} (Figure S1). The N−H stretch vibration at 3320 cm^{-1} of BPGa@COF-Cu further confirms the existence of the CO−NH bond in BPGa@COF-Cu. UV−vis spectra show five absorption bands of BPGa@COF in DMF at 427 nm (S-band), 524 nm (Q-band), 565 nm (Q-band), 600 nm (Q-band), and 657 nm (Q-band), indicating the existence of porphyrins (Figure 2). For BPGa@COF-Cu in DMF, the blue-shifted S band at 422 nm indicates the coordination of copper to porphyrin. The interaction of copper(II) with porphyrins was further confirmed by the blue shift absorptions in diffuse spectra. UV−vis-NIR diffuse reflection spectra data of BPGa@COF-Cu at 393, 457, 547, and 586 nm indicated the existence of metal-porphyrin and BP (Figure S2). The XRD pattern of BPGa@COF-Cu was compared with the standard BP card (JCPDS No. 73-1358). The diffraction peaks at 16.9°, 26.4°, and 34.1° correspond to the (020), (021), and (040) crystal planes of BP, respectively (Figure S3). Furthermore, nitrogen absorption−desorption isotherms of BPGa@COF-Cu were conducted and the results confirmed that BPGa@COF-Cu was constructed in the shape of a metal porphyrin-modified nanoball. The BET (Brunauer−Emmett−Teller) data show that the surface area of BPGa@COF-Cu is 17.40 m^2/g, with an average pore volume of 0.15 cm^3/g and pore size of 18.36 nm (Figure S4).

In Figure 3, XPS spectra of BPGa@COF-Cu confirmed the existence of C, N, O, P, Cu and Ga elements. The binding energy bands of C 1s at 288.1 and 286.0 eV were attributed to C═O and C−N bonds, respectively. The strong bands at 288.1 531.8, and 401.6 eV (Figure 3c) confirmed the formation of the CO-NH bond. The 398.5 eV in N 1s belongs to the C═N bonds of porphyrins, and 400.2 eV attributed to the N−Cu bond indicating the coordination of copper with porphyrins.[25] The main band at 133.7 eV (P 2p) belongs to P−O bonds due to the oxidation of BP (Figure 3e).[15] The Cu(II) $2p_{3/2}$ (or $2p_{1/2}$) bind energy peak is located at 935 eV (or 55.1 eV) (Figure 3f), indicating that Cu(II) are the main species formed in the compound. The satellite peaks at both 944.7 and 963.3 eV show there are some Cu(I) species in the compound may be due to the reduction of BP.

Photochemical Properties. To evaluate the photochemical properties, hydroxyl radicals (·OH) and singlet oxygen ($^1O_2$) were measured (Figure 4). 1,3-Diphenylisobenzofuran (DPBF) is a singlet oxygen quencher.[26] First, $^1O_2$ was detected by measuring the absorption change of DPBF at 415 nm. Both BPGa@COF and BPGa@COF-Cu generated singlet oxygen and decreased the absorption of DPBF at 415 nm by 30% (Figure 4b) and 60% (Figure 4c) upon red LED light

https://doi.org/10.1021/acsomega.4c00496
ACS Omega 2024, 9, 24513−24519

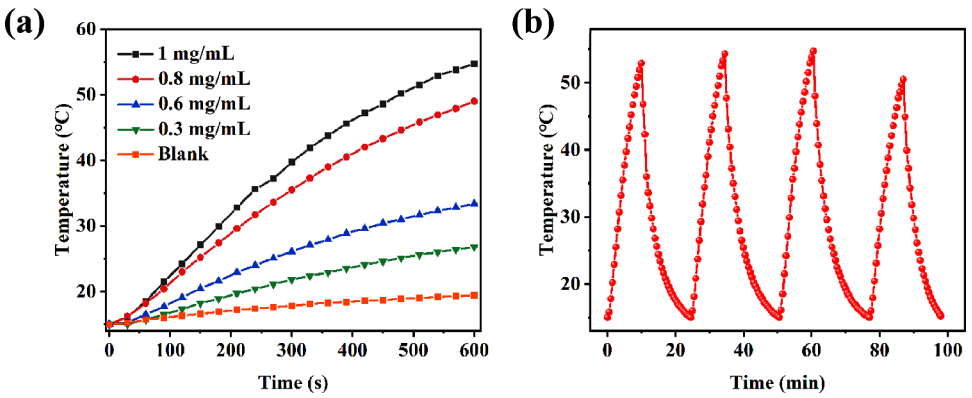

Figure 5. (a) Heating curves of BPGa@COF-Cu at different concentrations; (b) cyclic heating and cooling curves of BPGa@COF-Cu (1 mg/mL).

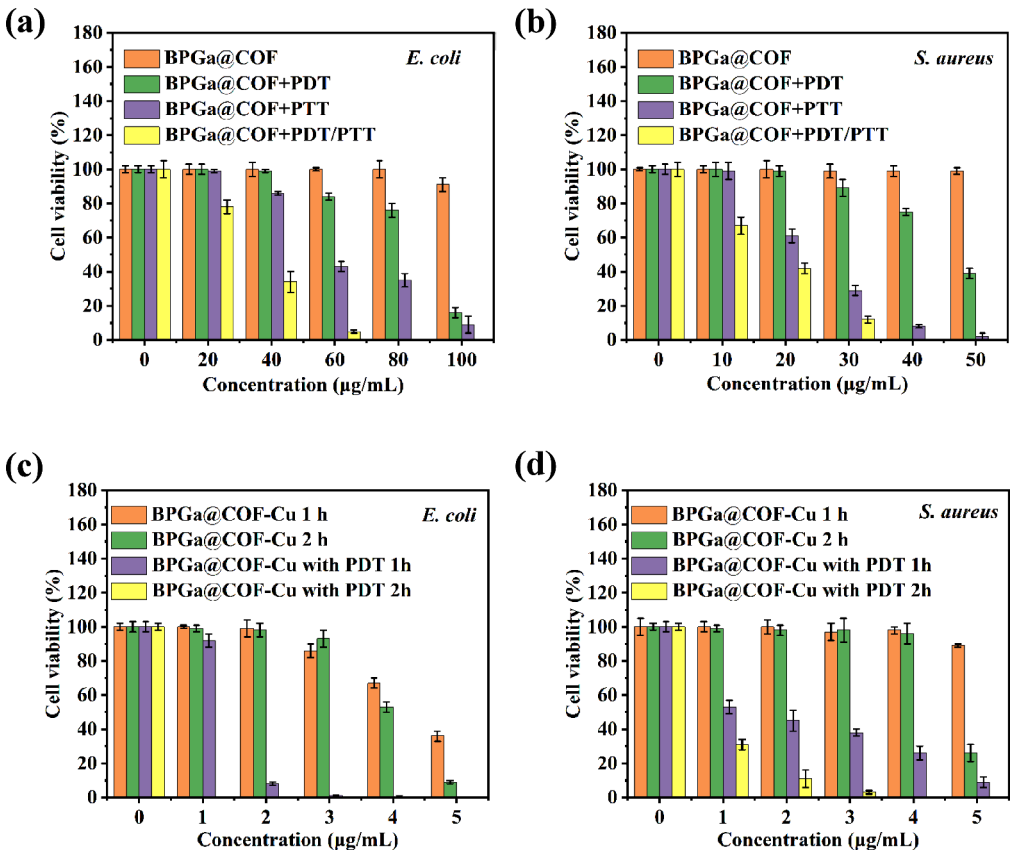

Figure 6. (A) Plots of bacterial viability (a, *E. coli*; b. *S. aureus*) by BPGa@COF without irradiation, under red-light irradiation (PDT), under NIR light irradiation (PTT), and under the synergistic effect of red and NIR light (PDT+PTT).(B) Plots of bacterial viability (c. *E. coli*; b. *S. aureus*) by BPGa@COF-Cu under dark- and red-light irradiation (PDT).

irradiation, which indicates that BPGa@COF-Cu is a good $^1O_2$ generator under irradiation.

To evaluate the effect of BPGa@COF-Cu on the catalyzed decomposition of H_2O_2, MB (Methylene blue trihydrate) was used to react with hydroxyl radicals (·OH) by recording the absorption change at 660 nm (Figure S5).[27] The absorption of MB at 660 nm was decreased from 1.0 to 0.6 (Figure S5b) while H_2O_2 has less effect, indicating the transfer of H_2O_2 into the ·OH (Fenton effect) catalyzed by BPGa@COF-Cu. Moreover, the absorption of MB at 660 nm disappeared due to the good photothermal effect and enhanced Fenton effect of BPGa@COF-Cu after irradiation by red LED light (Figure S5c).

The photothermal property of BPGa@COF-Cu was evaluated by 808 nm irradiation (Figure 5a). After irradiation for 10 min, In a blank aqueous solution, the temperature increment was marginal at 4.4 °C. However, with increasing concentrations, significant rises were observed: 11.8 °C at 0.3 mg/mL, 34 °C at 0.8 mg/mL, and a notable surge to 39.7 °C at 1 mg/mL (Figure 5a). As expected, the photothermal response of BPGa@COF-Cu is concentration-dependent, enhanced by the BPGa core's photothermal activity and Cu-porphyrin shell's thermal transfer. Cycling heating−cooling curves confirm its stable, recyclable photothermal properties (Figure 5b).

Antibacterial Inhibition. The inhibition effect against *E. coli* (or *S. aureus*) was assayed (Figures 6 and S6). The MIC of

https://doi.org/10.1021/acsomega.4c00496
ACS Omega 2024, 9, 24513−24519

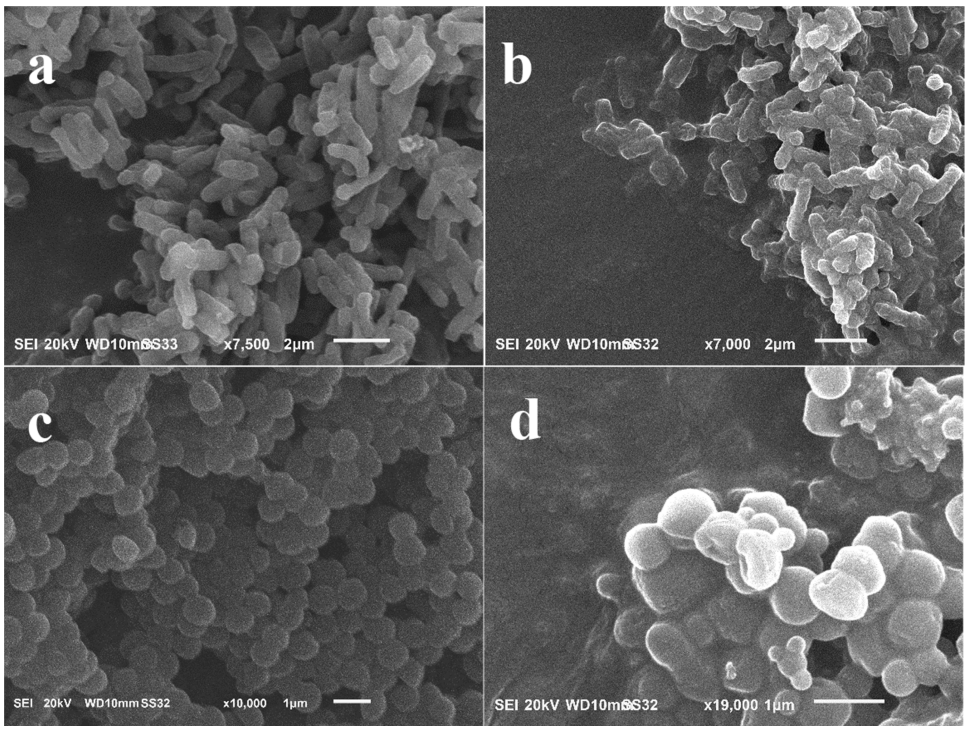

Figure 7. SEM images of *E. coli* untreated (a), *E. coli* treated by BPGa@COF-Cu with irradiation (b) and *S. aureus* untreated (c), *S. aureus* treated by BPGa@COF-Cu with irradiation (d).

BPGa@COF-Cu against *E. coli* was calculated as 5 μg/mL (without irradiation) and 1 μg/mL (with red LED light). While the MIC of BPGa@COF-Cu against *S. aureus* is calculated as 5 μg/mL (without irradiation) and 3 μg/mL (with red LED light). Without irradiation, the antibacterial activity may be in situ ·OH generation by the reaction of BPGa@COF-Cu and H_2O_2 (Fenton effect). Under NIR irradiation, the photo-driven generation of $^1O_2$ and photothermal PTT effect enable even low concentrations of BPGa@COF-Cu to exhibit exceptional antibacterial efficacy. The morphology changes of bacteria, before and after incubation with BPGa@COF-Cu, were observed by the SEM method (Figure 7). Live *E. coli* cells present a smooth surface and display a uniform and intact rod-like morphology, and live *S. aureus* cells are spherical in shape, characterized by uniformly full and even granules (Figure 7a,c). BPGa@COF-Cu made the cell membranes of bacteria shrink (Figure 7b,d) this suggests that BPGa@COF-Cu compromises the bacterial cell wall, resulting in bacterial cell death.

CONCLUSIONS

We herein report a metal−organic nanoball material BPGa@COF-Cu, which was synthesized by means of the CO-NH bond formation of TAPP and terephthalic chloride on the surface of BPGa species and the further coordination with Cu(II). The TEM data showed the mean radius of nanoballs is ca. 250 nm. The successful synthesis of COF in BPGa@COF-Cu was confirmed by the IR peak at 1667 cm^{-1} for the CO-NH stretch. The photothermal properties of BPGa@COF-Cu were then characterized, and the results show it is a good $^1O_2$ generator under irradiation, efficiently catalyzing H_2O_2 into the ·OH. These enhanced photothermal properties are thanks to the photothermal core BPGa and thermal transfer shell (Cu-porphyrin). The inhibition performance of BPGa@COF-Cu against *E. coli* and *S. aureus* was examined under red LED light, and the results show that the MIC are 1 and 3 μg/mL, respectively. Antibacterial inhibition data suggested that BPGa@COF-Cu made cell wall disruption and killed the bacteria, recommending BPGa@COF-Cu is a kind of LED light-enhanced nanoarchitectonics for bacterial treatment.

ASSOCIATED CONTENT

Supporting Information

The Supporting Information is available free of charge at https://pubs.acs.org/doi/10.1021/acsomega.4c00496.

FTIR spectra; UV−vis-NIR diffuse reflection spectra; nitrogen absorption−desorption isotherms; degradation curve of MB; and plate pictures of inhibition of bacteria (PDF)

AUTHOR INFORMATION

Corresponding Author

Qiu-Yun Chen − *School of Chemistry and Chemical Engineering, Jiangsu University, Zhenjiang 212013, People's Republic of China;* orcid.org/0000-0001-9708-5474; Email: chenqy@ujs.edu.cn

Authors

Jing-Jing Liu − *School of Chemistry and Chemical Engineering, Jiangsu University, Zhenjiang 212013, People's Republic of China*

Jun Wang − *School of Chemistry and Chemical Engineering, Jiangsu University, Zhenjiang 212013, People's Republic of China;* orcid.org/0009-0006-9992-7253

Feng Chen − *School of Chemistry and Chemical Engineering, Jiangsu University, Zhenjiang 212013, People's Republic of China*

https://doi.org/10.1021/acsomega.4c00496
ACS Omega 2024, 9, 24513−24519

Gao-Ji Wang − *School of Chemistry and Chemical Engineering, Jiangsu University, Zhenjiang 212013, People's Republic of China*

Complete contact information is available at: https://pubs.acs.org/10.1021/acsomega.4c00496

Notes

The authors declare no competing financial interest.

■ ACKNOWLEDGMENTS

The financial support of the National Natural Science Foundation of China (21571085 and 22207046), Natural Science Foundation of Jiangsu Province (BK20220528), China Postdoctoral Science Foundation (2022M711390), and Scientific Research Foundation for High-leveled Talents of Jiangsu University (5501310019) is gratefully acknowledged.

■ REFERENCES

(1) Sommer, M. O. A.; Munck, C.; Toft Kehler, R. V.; Andersson, D. I. Prediction of antibiotic resistance: time for a new preclinical paradigm? *Nat. Rev. Microbiol.* **2017**, *15*, 689−696.

(2) Souza, T. H. S.; Sarmento-Neto, J. F.; Souza, S. O.; Raposo, B. L.; Silva, B. P.; Borges, C. P. F.; Santos, B. S.; Filho, P. E. C.; Rebouças, J. S.; Fontes, A. Advances on antimicrobial photodynamic inactivation mediated by Zn(II) porphyrins. *J. Photochem. Photobiol., C* **2021**, *49*, No. 100454.

(3) Pan, T. N.; Tang, Y. Y.; Pang, E.; Zhao, S. J.; Tan, Q. X.; Wang, B. H.; Jin, S. G.; Song, X. Z.; Lan, M. H. Self-assembled Fe^{3+}-baicalin nanoparticles for combined photothermal and chemodynamic therapy. *ACS Appl. Nano Mater.* **2023**, *6*, 23595−23602.

(4) Si, Z. Y.; Pethe, K.; Chan-Park, M. B. Chemical basis of combination therapy to combat antibiotic resistance. *JACS Au.* **2023**, *3*, 276−292.

(5) Zhang, N.; Zheng, Y. H.; Wang, Z. L.; Liu, X. Y. Copper(II) based low molecular weight collagen fragments-chlorin e6 nanoparticles synergize anticancer and anti-bacteria. *J. Photochem. Photobiol., B* **2022**, *232*, No. 112473.

(6) Mu, W.; Chen, C.; Chen, Q. Y. Bacterium-sculpted porphyrin-protein-iron sulfide clusters for distinction and inhibition of staphylococcus aureus. *Langmuir* **2022**, *38*, 10385−10391.

(7) Choi, S. R.; Britigan, B. E.; Narayanasamy, P. Dual inhibition of klebsiella pneumon iae and pseudomonas aeruginosa iron metabolism using gallium porphyrin and gallium nitrate. *ACS Infect. Dis.* **2019**, *5*, 1559−1569.

(8) Zhao, S. S.; Guo, X. P.; Pan, X. H.; Huang, Y. B.; Cao, R. An "all in one" strategy to boost antibacterial phototherapy via porphyrin and boron dipyrromethenes based covalent organic framework. *Chem. Eng. J.* **2023**, *457*, No. 141017.

(9) Schlachter, A.; Asselin, P.; Harvey, P. D. Porphyrin-containing MOFs and COFs as heterogeneous photosensitizers for singlet oxygen-based antimicrobial nanodevices. *ACS Appl. Mater. Interfaces* **2021**, *13*, 26651−26672.

(10) Openda, Y. I.; Sen, P.; Managa, M.; Nyokong, T. Acetophenone substituted phthalocyanines and their graphene quantum dots conjugates as photosensitizers for photodynamic antimicrobial chemotherapy against staphylococcus aureus. *Photodiagn. Photodyn. Ther.* **2020**, *29*, No. 101607.

(11) Zhang, H.; Li, Q. S.; Qi, X. Y.; Li, Y.; Ma, H. Y.; Grinholc, M.; Nakonieczna, J.; Yu, B. R.; Wang, X.; Zhang, L. Iron-blocking antibacterial therapy with cationic heme-mimetic gallium porphyrin photosensitizer for combating antibiotic resistance and enhancing photodynamic antibacterial activity. *Chem. Eng. J.* **2023**, *451*, No. 138261.

(12) Park, J. O.; Tanner, L. B.; Wei, M. H.; Khana, D. B.; Jacobson, T. B.; Zhang, Z.; Rabinowitz, J. D. Near-Equilibrium Glycolysis Supports Metabolic Homeostasis and Energy Yield. *Nat. Chem. Biol.* **2019**, *15*, 1001−1008.

(13) Bhusal, R. P.; Bashiri, G.; Kwai, B. X. C.; Sperry, J.; Leung, I. K. H. Targeting isocitrate lyase for the treatment of latent tuberculosis. *Drug Discov Today.* **2017**, *22*, 1008−1016.

(14) Matsumoto, Y.; Nakashima, T.; Cho, O.; Ohkubo, T.; Kato, J.; Sugita, T. Pyruvate-triggered TCA cycle regulation in Staphylococcus aureus promotes tolerance to betamethasone valerate. *Biochem. Biophys. Res. Commun.* **2020**, *528*, 318−321.

(15) Wang, J.; Chen, F.; Chen, Q. Y.; Wang, G. J. Europium and black phosphorus-functionalized porphyrin as an L-arginine sensor and L-arginine activated pdt/ptt agent for bacteria treatment. *ACS Appl. Mater. Interfaces* **2023**, *15*, 41861−41869.

(16) Yang, S. P.; Shao, Y. Q.; Sun, Y. Y.; He, Z. L.; Wang, Y.; Zhai, Y. N.; Dong, Y. B.; Feng, J. Covalent organic framework-based nanomotor for multimodal cancer photo-theranostics. *Adv. Healthcare Mater.* **2023**, *12*, No. 2301645.

(17) Ran, P.; Chen, W. J.; Zheng, H.; Zhou, J. J.; Qiu, B.; Cao, W. X.; Li, X. H. Surface decoration of black phosphorus nanosheets to generate oxygen and release $^1O_2$ for photodynamic killing of bacteria. *Nanoscale* **2021**, *13*, 13506−13518.

(18) Wang, J.; Wu, K.; Chen, C. H.; Chen, Q. Y.; Liu, Q. S. Composite nanoarchitectonics of cellulose with porphyrin-Zn for antibacterial properties. *J. Inorg. Organomet. Polym. Mater.* **2023**, *33*, 207−215.

(19) Ariga, K. Nanoarchitectonics: what's coming next after nanotechnology? *Nanoscale Horiz.* **2021**, *6*, 364−378.

(20) Mu, W. Y.; Wang, J.; Chen, Q. Y. Metal porphyrin array modifed cellulose terephthalate for sustainable bacterial absorption and sterilization. *Cellulose* **2023**, *30*, 5845−5856.

(21) Liu, W. X.; Xiao, D. X.; Tao, Z. F.; Dong, A. Europium and glycopolymer-modified silica nanoparticles on black phosphorus nanosheets for bacterial targeting, imaging, and ablation. *ACS Appl. Nano Mater.* **2022**, *5*, 11948−11955.

(22) Liang, H. H.; Zhang, K. Q.; Wang, Y. D.; Song, X. M.; Tao, A. Y.; Liu, Y. Z.; Jin, Z. 2D layered black arsenic-phosphorus materials: synthesis, properties, and device applications. *Nano Res.* **2022**, *15* (4), 3737−3752.

(23) Zhao, S.; Wang, Z. P.; Lin, Z. H.; Wei, G. X.; Wen, X. M.; Li, S. Y.; Yang, X. H.; Zhang, Q.; Jing, C. M.; Dai, Y. W.; Guo, J.; He, Y. Drug repurposing by siderophore conjugation: synthesis and biological evaluation of siderophore-methotrexate conjugates as antibiotics. *Angew. Chem., Int. Ed.* **2022**, *61*, No. e202204139.

(24) Chen, T.; Zeng, W. W.; Tie, C. J.; Yu, M.; Hao, H. S.; Deng, Y.; Li, Q. Q.; Zheng, H. R.; Wu, M. Y.; Mei, L. Engibeered gold/black phosphorus nanoplatforms with remodeling tumor microenvironment for sonoactivated catalytic tumor theranostics. *Bioactive Mater.* **2022**, *10*, 515−525.

(25) He, C. H.; Liu, C.; Li, M. Y.; Li, M.; Yin, J. L.; Han, S. M.; Xia, J.; Chen, D. Y.; Cao, W. B.; Lu, Q. P.; Rosei, F. 3D hierarchical Cu-MOF nanosheets-based antibacterial mesh. *Chem. Eng. J.* **2022**, *446*, No. 137381.

(26) Lu, J. Y.; Zhang, P. L.; Chen, Q. Y. A Nano-BODIPY encapsulated zeolitic imidazolate framework as photoresponsive integrating antibacterial agent. *ACS Appl. Bio Mater.* **2020**, *3*, 458−465.

(27) Mu, W. Y.; Wang, W.; Chen, Q. Y.; Qu, L. L. Polymer fused GOFe: Light-driven oxygen donor and antiseptics. *J. Photochem. Photobiol. A: Chem.* **2021**, *408*, No. 113075.